

Inverse Compton emission from relativistic particles accelerated at shear layers in relativistic jets

Tej Bahadur Chand (North-West University, Potchefstroom, South Africa)
Markus Böttcher (North-West University, Potchefstroom, South Africa)



chandtej11@gmail.com

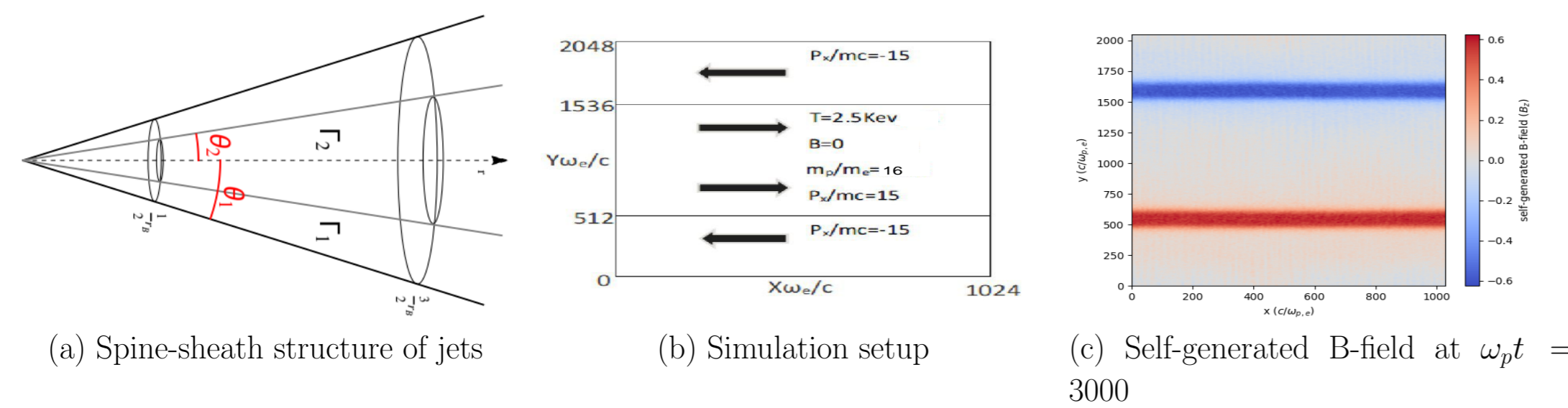


Abstract

Both observational evidence as well as theoretical considerations from MHD simulations of jets suggest that the relativistic jets of active galactic nuclei (AGN) are radially stratified, with a fast inner spine surrounded by a slower-moving outer sheath. The resulting relativistic shear layers are a prime candidate for the site of relativistic particle acceleration in the jets of AGN and gamma ray bursts (GRBs). We present results of particle-in-cell simulations of magnetic-field generation and particle acceleration in the relativistic shear boundary layers (SBLs) of jets in AGN and GRBs including the self-consistent calculation of the radiation spectrum produced by inverse Compton scattering of relativistic electrons in an external soft photon field.

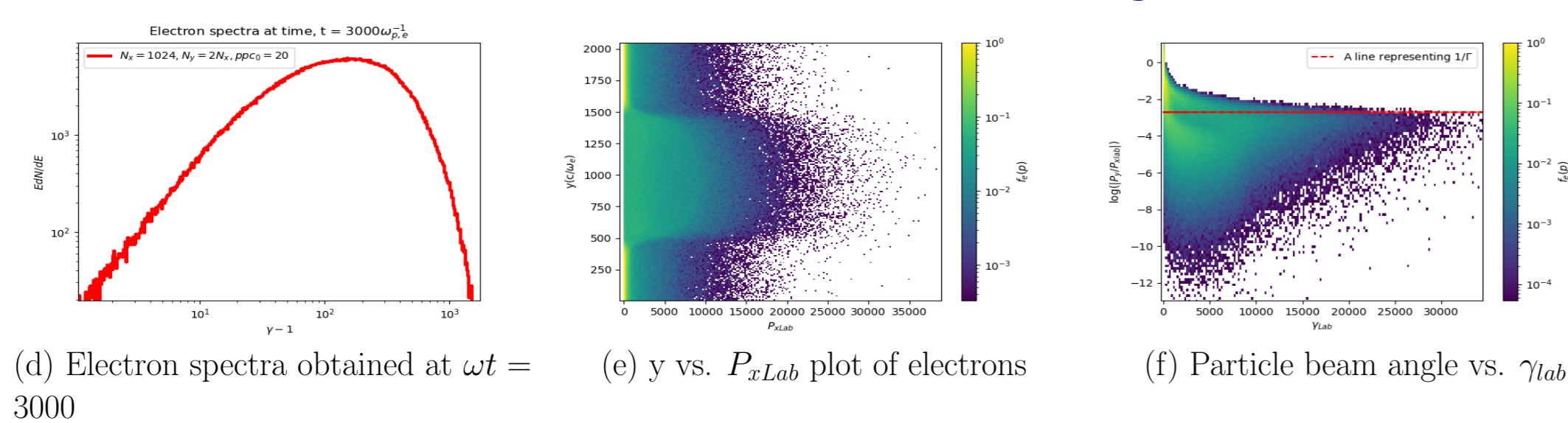
Spine-sheath Morphology of Relativistic Jets

- Relativistic jets are **collimated outflows** of matter from the **accreting black holes** residing at the centre of the active galaxies (AGN) that can travel undisrupted over kpc scales.
- Spine-sheath structures of relativistic jets (see fig (a)), with **fast-moving inner spine** surrounded by the **slow-moving sheath** have been investigated both observationally and theoretically (Ghisellini et al., 2005). The shear layers formed in the relativistic jets are promising sites for particle acceleration (Alves & et al., 2012; Liang et al., 2013a).
- Particle-in-Cell (PiC) simulations of the pure e^- -ion plasma, initially unmagnetized, self-generates magnetic fields due to plasma instabilities (e.g. Weibel instability), which eventually leads to particle energization. For this, we used the TRISTAN-MP code developed by Anatoly Spitkovsky (2005).



In the simulation setup (see fig (b)), the spine and sheath propagate with the equal bulk Lorentz factor ($\Gamma = 15$) but in an opposite direction from each other. All simulations are performed in the **equal Lorentz factor frame (ELF)**, which moves with respect to the observer's frame (lab frame) with Lorentz factor Γ . The plasma temperature is 2.5 keV and the ion to electron mass ratio is $m_i/m_e = 16$. The simulation box in xy -plane has grid points 1024 and 2048 along x and y axes. SBLs are formed at $y = 512$ and $y = 1536$. The spatial distances are measured in plasma skin depth while the time is measured in $1/\omega_p$. Value of speed of light is set $c = 0.45\Delta x/\Delta t$ to fulfil the Courant condition. From the simulations, the self-generated magnetic field is developed along z -axis (see fig.(c)).

Particle Spectra & Anisotropy



- The electron spectrum peaks around $\gamma_{max} \approx \frac{1}{2} \frac{\gamma_i m_i}{m_e}$. Diffusion of some spine electrons to the sheath region takes place.
- All high energy spine electrons have beam angles much smaller than $1/\Gamma$, where Γ is the bulk Lorentz factor of the plasma. There exists an anticorrelation between beam angle and e^- -energy.

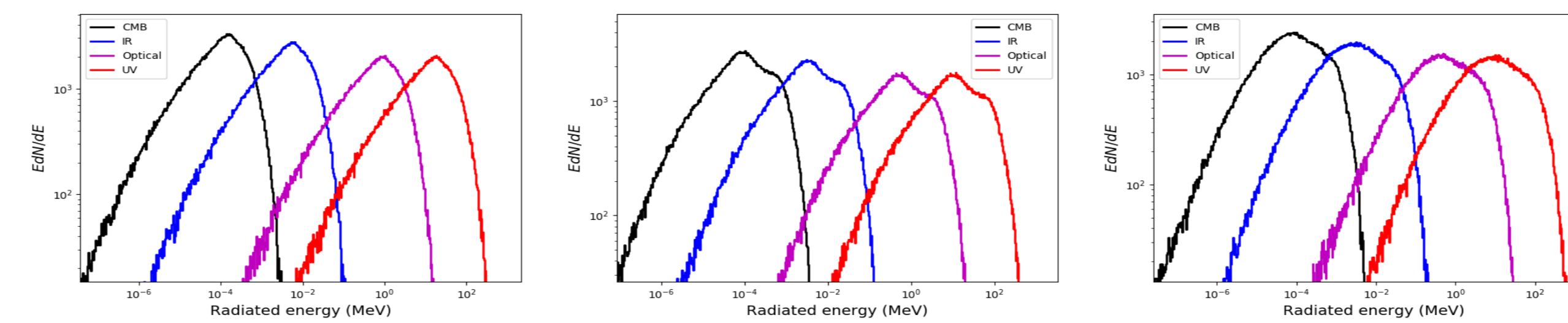
Angle-independent Radiation Spectra

We evaluate electron cooling term assuming a thermal blackbody external radiation field of different temper-

atures and thus wavelength regimes. Radiation spectra are evaluated using a simple **delta-function approximation** for the target photon field. The radiation cooling term for inverse Compton scattering of relativistic electrons in the external photon field in the Thomson regime is:

$$\left(\frac{d\gamma}{dt}\right)_{rad} = \frac{\pi^4}{15} \sigma_T c K \gamma^2 \theta^4, \quad K = \frac{8\pi}{\lambda_c^3}, \quad \theta = \frac{K_B T}{m_e c^2}, \quad \sigma_T \text{ is Thomson cross-section.} \quad (1)$$

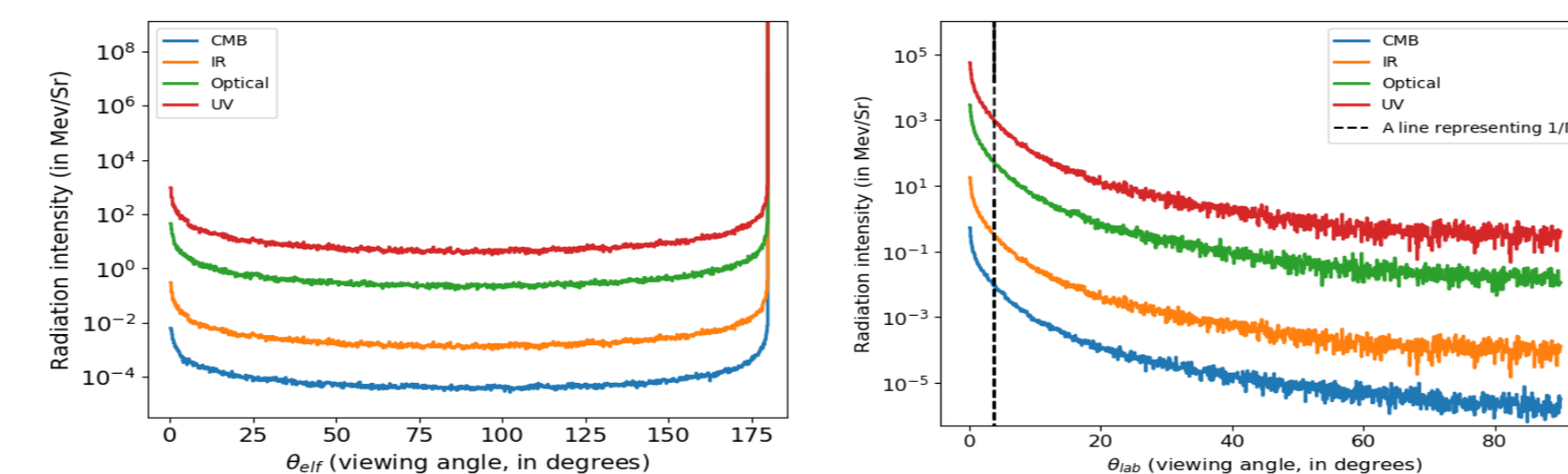
The **angle-integrated** radiation spectra for different radiation temperatures obtained from the PiC simulations are shown in figures (g), (h) and (i).



(g) Radiation spectra obtained at $\omega_p t = 1500$ (h) Radiation spectra obtained at $\omega_p t = 2500$ (i) Radiation spectra obtained at $\omega_p t = 3000$

- As the simulations progress, a single component quasi-thermal radiation spectrum develops into a two-component spectrum that eventually becomes a quasi-thermal low-frequency spectrum with a cut-off power-law tail.

For the observation of the radiative output, the frequency-integrated radiation intensity is plotted as a function of the viewing angle (an angle between the direction along which the observer observes the radiation with the jet axis).



(j) Intensity vs. viewing angle in ELF frame at $\omega_p t = 3000$ (k) Intensity vs. viewing angle in the lab frame at $\omega_p t = 3000$

- In the ELF frame, highest radiation intensity is observed along the jet axis ($\theta_{ELF} = 0^\circ$ & $\theta = 180^\circ$).
- In the lab. frame, the radiation is strongly beamed in the forward direction, with a characteristic opening angle $\approx 1/\Gamma$.

Angle-dependent Radiation Spectra

In the case of Compton scattering by ultra-relativistic electrons ($\gamma \gg 1$), all scattered photons will travel in the direction of the incoming electron (Boettcher & Krawczynski, 2012). Hence the Compton cross section can be approximated as $\frac{d\sigma_C}{d\Omega_s d\epsilon_s} = \delta(\Omega_s - \Omega_e) \frac{d\sigma_C}{d\epsilon_s}$, where Ω_s & Ω_e denote directions of photons and electrons.

$$\frac{d\sigma_C}{d\Omega_s d\epsilon_s} = \frac{\pi r_e^2}{\gamma \epsilon'} \left\{ y + \frac{1}{y} - \frac{2\epsilon_s}{\gamma \epsilon' y} + \left(\frac{\epsilon_s}{\gamma \epsilon' y} \right)^2 \right\} H \left(\epsilon_s; \frac{\epsilon'}{2\gamma}, \frac{2\gamma \epsilon'}{1+2\epsilon'} \right) \quad (\text{Boettcher \& Krawczynski, 2012})$$

Here, $y = 1 - \frac{\epsilon_s}{\gamma}$ and $\epsilon' = \gamma \epsilon (1 - \beta \mu)$. The Compton emissivity can be written as:

$$j(\epsilon, \gamma, \mu) = \frac{3m_e c^3 \sigma_T \epsilon_s}{8\gamma} \int_0^\infty \frac{1}{\epsilon'} \left\{ y + \frac{1}{y} - \frac{2\epsilon_s}{\gamma \epsilon' y} + \left(\frac{\epsilon_s}{\gamma \epsilon' y} \right)^2 \right\} n_{ph}(\epsilon, \theta) H \left(\epsilon_s; \frac{\epsilon'}{2\gamma}, \frac{2\gamma \epsilon'}{1+2\epsilon'} \right) d\epsilon$$

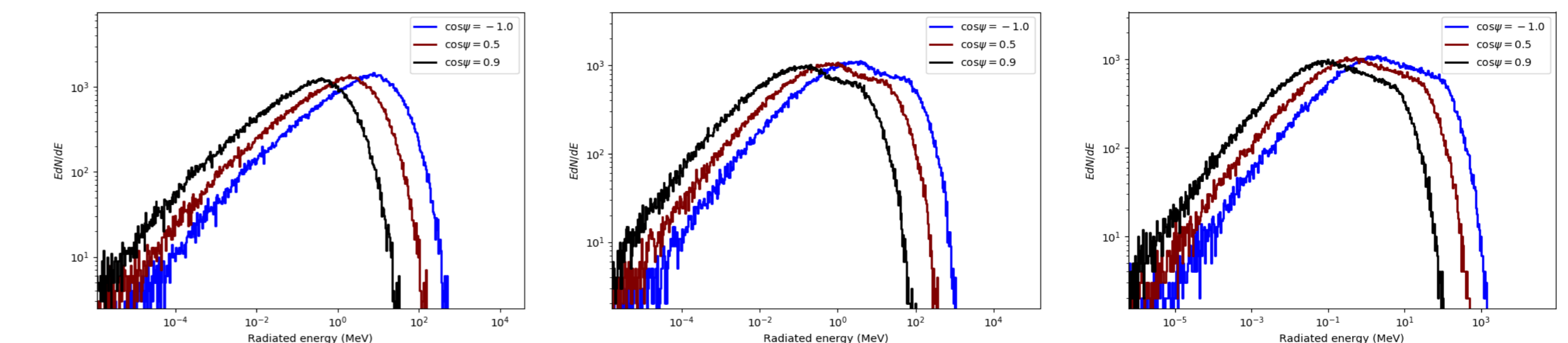
Where, $n_{ph}(\epsilon, \theta)$ is photon density. The blackbody radiation field is strongly peaked near photon energies $\epsilon \cong \theta$. So, a **monochromatic δ -function approximation** can provide sufficient accuracy for spectral calculation. Hence, $n_{ph}(\epsilon, \theta) = n_{ph}(\theta) \delta(\epsilon - \theta)$ Where, $n_{ph}(\theta) = K \theta^3 \Gamma(3) \zeta(3) = 2.4K \theta^3$.

So, the cooling term for inverse Compton scattering of relativistic electrons in angle-dependent photon field in the Thomson regime is:

$$\frac{d\gamma}{dt}(\mu, \gamma, \theta) = \frac{2.4 \times 3c\sigma_T K \theta^2}{2.7 \times 8\gamma^2 (1 - \beta\mu)} \left[(\epsilon_{smax}^2 - \epsilon_{smin}^2) + \frac{\epsilon_{smax}^4 - \epsilon_{smin}^4}{4\gamma^2} + \frac{\epsilon_{smax}^5 - \epsilon_{smin}^5}{5\gamma^3} - \frac{2}{2.7\theta(1 - \beta\mu)} \left\{ \frac{(\epsilon_{smax}^3 - \epsilon_{smin}^3)}{3\gamma^2} + \frac{\epsilon_{smax}^4 - \epsilon_{smin}^4}{4\gamma^3} \right\} + \frac{1}{\gamma^4 (2.7\theta)^2 (1 - \beta\mu)^2} \left\{ \frac{\epsilon_{smax}^4 - \epsilon_{smin}^4}{4} + \frac{2(\epsilon_{smax}^5 - \epsilon_{smin}^5)}{5\gamma} + \frac{\epsilon_{smax}^6 - \epsilon_{smin}^6}{2\gamma^2} + \frac{4(\epsilon_{smax}^7 - \epsilon_{smin}^7)}{7\gamma^3} \right\} \right] \quad (2)$$

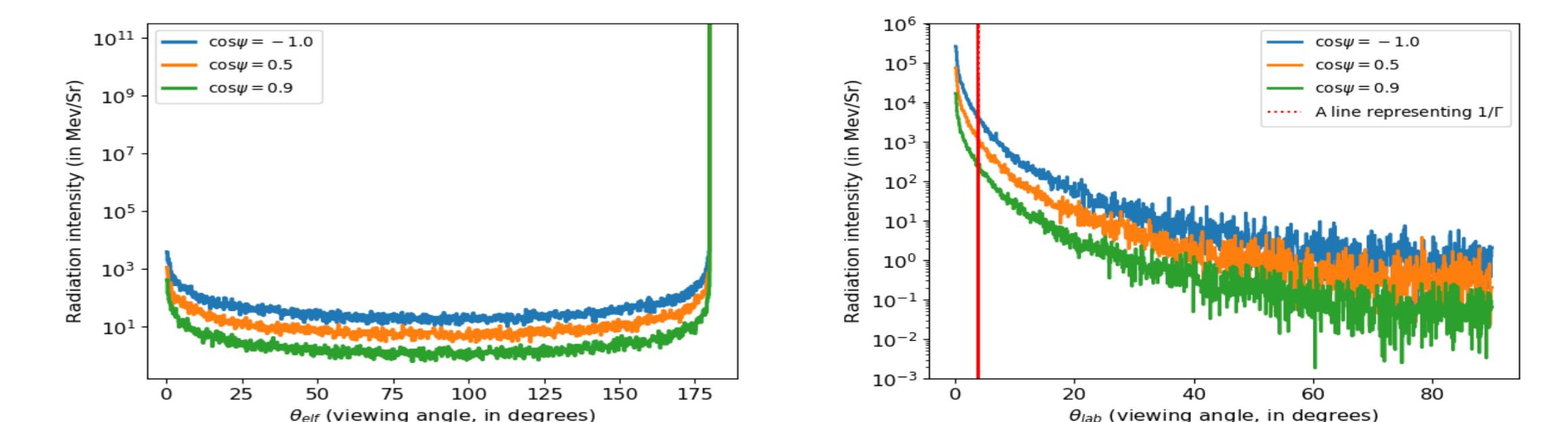
where $\epsilon_{smax} = \frac{5.4\gamma^2(1-\beta\mu)\theta}{1+5.4\gamma\theta(1-\beta\mu)}$ and $\epsilon_{smin} = \frac{2.7\theta(1-\beta\mu)}{2}$ and $\mu = \cos \psi$. ψ is the angle between directions of propagation of interacting photon and electron.

- The radiation spectra due to inverse Compton scattering of relativistic electrons in an angle-dependent **UV-photon field** are given below.
- The scattered photon energy is maximum for head-on collisions ($\cos \psi = -1$) and decreases for smaller scattering angles, as expected.



(l) Radiation spectra obtained at $\omega_p t = 2000$ (m) Radiation spectra obtained at $\omega_p t = 4000$ (n) Radiation spectra obtained at $\omega_p t = 5000$

- The angle dependence of the radiation intensity, taking into account angle-dependent electron cooling, is illustrated in Figures (o) and (p) below.
- As in the case of angle-independent electron cooling, the emitted radiation is strongly boosted along the jet axis, with a characteristic opening angle $1/\Gamma$. This boosting, stronger than expected from Doppler boosting of an intrinsically isotropic radiation field in the co-moving frame of the spine, may resolve the long-standing problem of the Doppler factor crisis (Lyutikov & Lister, 2010).



(o) Intensity vs. viewing angle in equal Lorentz factor frame (p) Intensity vs. viewing angle in the laboratory frame

References

- Alves, E.P., Grismayar, T., Martins S.F., et al.: 2012, 746, L14, doi: 10.1088/2041-8205/746/2/114
 Boettcher, M., Harris, D.E. & Krawczynski H.: 2012, Relativistic Jets from Active Galactic Nuclei
 Ghisellini, G., Tavecchio, F.: 2005, A&A, 432, 401, doi: 10.1051/0004-6361:20041404
 Liang, E., Boettcher, M. & Smith I.: 2013a, The Astrophysical Journal, 766, L19, doi: 10.1088/2041-8205/766/2/L19
 Lyutikov, M., & Lister, M.: 2010, The Astrophysical Journal, 722, 197, doi: 10.1088/0004-637x/722/1/197
 Spitkovsky, A.: 2005, AIP Conference Proceedings, 500 doi: 10.1063/1.2141897